CHINESE OPTICS LETTERS
Vol. 19, No. 12 | December 2021

Q-switched mode-locked multimode fiber laser based on a graphene-deposited multimode microfiber

Jia-Wen Wu (吴家文)[1], Yu-Xin Gao (高玉欣)[2], Xu-Bin Lin (林旭斌)[1], Jin-Gan Long (龙金干)[1], Hu Cui (崔 虎)[1], Zhi-Chao Luo (罗智超)[1], Wen-Cheng Xu (徐文成)[1], and Ai-Ping Luo (罗爱平)[1*]
[1] Guangdong Provincial Key Laboratory of Nanophotonic Functional Materials and Devices, South China Normal University, Guangzhou 510006, China
[2] Department of Mechanical and Electrical Engineering, Shandong Polytechnic College, Jining 272067, China

*Corresponding author: luoaiping@scnu.edu.cn
Received April 19, 2021 | Accepted June 4, 2021 | Posted Online September 15, 2021

We report Q-switched mode-locked (QML) pulses generation in an Yb-doped multimode fiber (MMF) laser by using a graphene-deposited multimode microfiber (GMM) for the first time, to the best of our knowledge. The single-wavelength QML operation with the central wavelength tunable from 1028.81 nm to 1039.20 nm and the dual-wavelength QML operation with the wavelength spacing tunable from 0.93 nm to 5.79 nm are achieved due to the multimode interference filtering effect induced by the few-mode fiber and MMF structure and the GMM in the cavity. Particularly, in the single-wavelength QML operation, the fifth harmonic is also realized owing to the high nonlinear effect of the GMM. The obtained results indicate that the QML pulses can be generated in the MMF laser, and such a flexible tunable laser has promising applications in optical sensing, measuring, and laser processing.

Keywords: Q-switched mode-locked pulse; graphene-deposited multimode microfiber; multimode fiber laser.
DOI: 10.3788/COL202119.121402

1. Introduction

Nowadays, the multimode fiber (MMF), which was overlooked for decades, is making a strong comeback since it can address plenty of long-standing issues relating to the single-mode fiber (SMF). For optical communication, based on the spatial division multiplexing technique[1,2], MMF can enhance the transmission capacity through adding the mode degree of freedom. In addition, MMF can meet the ever-increasing demands for high power laser[3] through increasing the mode area to reduce the nonlinear effects. Apart from the afore-mentioned applications, MMF also can be applied in imaging[4,5], metrology[6], quantum processing[7], and spectroscopy[8], to name a few. Meanwhile, MMF is also an ideal platform to investigate the complex nonlinear phenomena due to interaction between the transverse modes, such as ultrabroadband dispersive waves generation[9,10], geometric parametric instability[11–13], supercontinuum generation[14–16], spatiotemporal light beam compression[17], and beam self-cleaning[18–22].

As for the application of the MMF in high power lasers, it was mainly limited to the continuous wave (CW) laser in the past[23,24]. Recently, Wright *et al.* demonstrated a three-dimensional (3D) mode-locked laser using the MMF[25]. Compared with the conventional SMF laser, the 3D MMF laser locks many transverse modes and longitudinal modes synchronously, which is called a spatiotemporal mode-locked (STML) laser owing to the increase of the transverse mode freedom. With the development of the research on STML MMF lasers, it is found that the temporal characteristics of the STML pulses are similar to those of SMF lasers including the single pulse[26–28], multi-pulse[29,30], and self-similar pulse[31], except for the complex beam spot. These investigations focus on the continuous mode-locked pulses. In fact, there are two other special types of pulses in lasers, namely Q-switched and Q-switched mode-locked (QML) pulses. Very recently, Q-switched pulses were achieved in the MMF laser[32]. Then, it naturally leads to a question: is it possible to generate QML pulses in the MMF laser? Up to now, it has not been reported.

In the QML operation state, the pulse-train is a continuous pulse-train modulated periodically by a Q-switched envelope. It can be seen as the transition state between the Q-switched state and the continuous mode-locked state. Therefore, QML pulses have characteristics of both Q-switched pulses and continuous mode-locked pulses. Compared to continuous mode-locked fiber lasers[33,34], QML fiber lasers can generate the pulses with higher pulse energy and tunable repetition rate[35]. Therefore, QML fiber lasers have been applied intensively in remote sensing, range finding, medicine, and laser processing. To obtain the QML pulses, both actively Q-switched technologies[36] and passively Q-switched technologies[35] have been employed in the SMF lasers. Generally speaking, the passively Q-switched technique with the saturable absorber is simpler and cheaper. Thus, it is interesting to know whether the QML pulses could be generated by employing the Q-switched technologies in the MMF lasers.

In this work, we address this issue. By constructing an Yb-doped MMF laser with a graphene-deposited multimode microfiber (GMM), the QML pulses are obtained. The single-wavelength QML operation in the MMF laser is firstly realized, and the central wavelength can be tuned from 1028.81 nm to 1039.20 nm. Particularly, we observe the generation of the fifth harmonic in the QML operation. In addition, the MMF laser can operate at the dual-wavelength QML state due to the filtering effect induced by the few-mode fiber and MMF structure and the GMM in the cavity. Furthermore, the dual-wavelength spacing can be tuned from 0.93 nm to 5.79 nm. The obtained results demonstrate that the QML pulses can be obtained in the MMF laser, and such a flexible laser with tunable wavelength would be helpful in applications of optical sensing, measuring, and laser processing.

2. Experimental Setup

The schematic of the proposed MMF laser is shown in Fig. 1. The gain fiber is a piece of ~2 m long double-cladding Yb-doped fiber (YDF, Liekki Yb1200-10/125 DC, core NA = 0.08, cladding NA > 0.46) and pumped by a 980 nm laser diode through a customized combiner with 10/125 μm fiber pigtails with the core NA of 0.08 and the cladding NA of 0.46. The YDF supports three transvers modes. The GMM is incorporated into the cavity to realize the QML operation. A polarization-independent isolator (PI-ISO) is used to ensure the unidirectional light propagation in the laser cavity. Two polarization controllers (PCs) are employed to optimize the operation state of the laser by adjusting the polarization state of the light. The laser is taken out for measuring by an optical coupler (OC) with an output ratio of 10%. Except for the YDF and the fiber pigtails of the combiner being few-mode fibers, all other fibers including the pigtails of

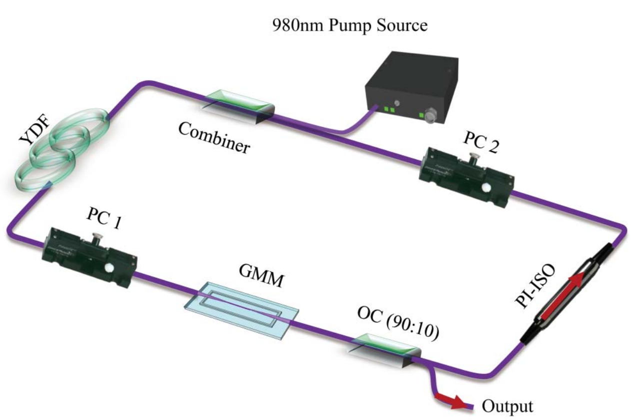

Fig. 1. Experimental setup of the QML MMF laser with a GMM.

the PI-ISO and the 90:10 OC in the cavity are conventional graded-index MMFs (Corning, 62.5/125 μm, NA = 0.275). The splice between the MMF and the few-mode fiber is completed by an arc fusion splicer. Due to the mismatch of the NAs, the splice loss for the light propagating from the passive few-mode fiber to the MMF is different from that of light propagating from the MMF to the passive few-mode fiber, which is ~8.21 dB and ~1.56 dB, respectively. The total length of the cavity is 16.9 m. We fasten all of the fibers on the optical table to maintain stable laser operation. The laser optical spectrum and frequency spectrum are measured by an optical spectrum analyzer (OSA, Yokogawa, AQ6317C) and a radio-frequency (RF) spectrum analyzer (Agilent, E4407B ESA-E SERIES, 26.5 GHz), respectively. An oscilloscope (Tektronix, DSA70804, 8 GHz) together with a photodetector (Newport, 1623 InGaAs nanosecond optical detector, 500 MHz) is used to measure the pulse-train. Moreover, a charge-coupled device (CCD) camera (Goldeye G-033SWIRTEC1) is used to measure the beam profile.

As the key component for achieving the QML operation, the GMM incorporated in the cavity is firstly fabricated through the following steps. Firstly, the multimode microfiber with a waist diameter of 6.73 μm, a waist length of 2.3 cm, and a loss of ~0.14 dB is made from the conventional graded-index MMF (Corning, 62.5/125 μm, NA = 0.275) by the flame brushing technique. Then, the multimode microfiber is transferred to a glass slide for depositing the graphene. For the purpose of uniformity, the graphene/dimethylformamide (DMF) solution with a concentration of 0.05 mg/mL, which will be dropped onto the multimode microfiber during the process of the deposition, is ultrasonicated for 30 min. After that, the optical deposition method described in Ref. [37] is employed. The process of the deposition is *in situ* observed through a microscope. The amount of the graphene deposited on the multimode microfiber can be controlled by adjusting the light power and the deposition time. In addition, the loss induced by the deposition is monitored by a power meter. The GMM with a deposition length of ~97 μm used in our experiment is shown in Fig. 2(a).

To further investigate the features of the fabricated GMM, we measure its nonlinear absorption by a balanced twin detector measurement technology. The light source used in the measurement is an in-house made picosecond pulse MMF laser (central wavelength, 1070 nm; repetition rate, 13.60 MHz). To control the input power of the GMM, a variable attenuator is used. The nonlinear transmission curve and the fitting curve of the GMM are illustrated in Fig. 2(b). As can be seen from Fig. 2(b), the fabricated GMM has the saturable absorption effect. The modulation depth is ~37.9%, and the non-saturable loss is ~46%. The modulation depth could be increased, and the non-saturable loss could be decreased by optimizing the deposition amount of the graphene. Such a large modulation depth and a large non-saturable loss are conducive to the generation of QML pulses. In addition to the saturable absorption effect, the GMM also has a filtering effect, as illustrated in Fig. 2(c), which is mainly formed by multimode interference in the taper's waist region[38].

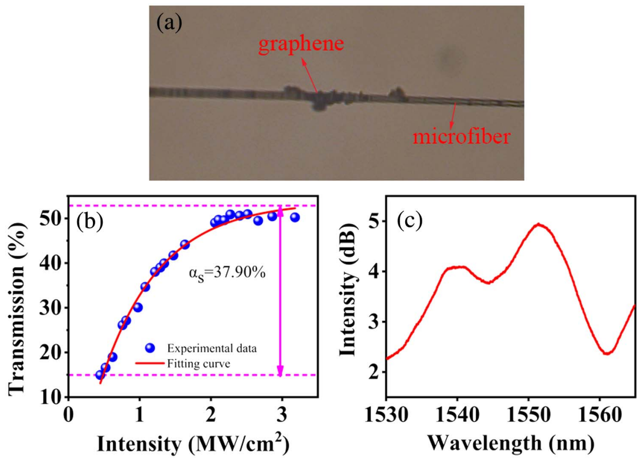

Fig. 2. (a) Microscope image of the fabricated GMM; (b) nonlinear saturable absorption curve and the corresponding fitting curve of the fabricated GMM; (c) spectral filtering characteristic of the fabricated GMM.

3. Experimental Results and Discussions

3.1 Single-wavelength QML operation

In our experiment, the CW operation is firstly achieved at the pump power of ~1.10 W. Then, by slightly increasing the pump power to ~1.14 W, the QML operation is realized. Figure 3 presents the characteristics of the typical QML operation at the pump power of 1.40 W. Figure 3(a) displays the QML pulse-train with the repetition rate of 16.04 kHz. In order to demonstrate more details of the QML pulses, it is enlarged and shown in Figs. 3(b) and 3(c). The envelope width of the QML pulses is 8.14 μs. The corresponding mode-locked pulses underneath the *Q*-switched envelope have the repetition rate of 11.58 MHz, corresponding to the light round-trip time in the cavity. The optical spectrum is presented in Fig. 3(d), where the central wavelength locates at 1039.20 nm. Figure 3(e) displays the RF spectrum, which has multiple peaks with an interval of 16.04 kHz, in accordance with the repetition rate of the *Q*-switched pulse envelope. The corresponding beam profile shown in Fig. 3(f) exhibits a speckle spatial pattern, similar to those in STML MMF lasers[25,26,28–31,39].

Moreover, due to the filtering effect induced by the few-mode fiber (the gain fiber and the matched passive fiber of the combiner) and the MMF structure[39], the wavelength-tunable QML operation is achieved by adjusting the two PCs. Figure 4 presents the optical spectra of the stable wavelength-tunable QML operation at the pump power of 1.40 W. The central wavelength of the QML pulses can be tuned from 1028.81 nm to 1039.20 nm, and the corresponding QML operation remains stable in the tuning process. Note that during the wavelength tuning process, the spectral intensities vary, due to the differences of the loss and gain at different wavelengths. Besides, satellite peaks in the spectrum are observed, as shown in Fig. 4, which could be ascribed to the multiple pass bands of the filter based on the few-mode fiber and MMF structure and the GMM. Nevertheless, the gain at these wavelengths is too low to form QML pulses.

Then, to further explore the characteristics of the QML operation, we investigate the evolution of the QML pulses at the central wavelength of 1034.80 nm by fixing the PCs and only adjusting the pump power. With the pump power increasing, it is found that the time interval between the adjacent *Q*-switched envelopes becomes shorter, as illustrated in Fig. 5(a). Figure 5(b) shows the repetition rate and the *Q*-switched pulse envelope width as a function of the pump power. The repetition rate increases monotonously from 18.19 kHz to 27.67 kHz, and the pulse envelope width decreases monotonously from 9.55 μs to 3.43 μs when the pump power increases from 1.30 W to 1.60 W, which are the typical characteristics of the QML operation. It can be interpreted that the time required to accumulate and release enough energy becomes shorter when the pump power increases. The pulse envelope width may be further shortened by reducing the length of the laser cavity[40], increasing the modulation depth of the saturable absorber, and optimizing the output ratio[41] as those demonstrated in SMF lasers. In

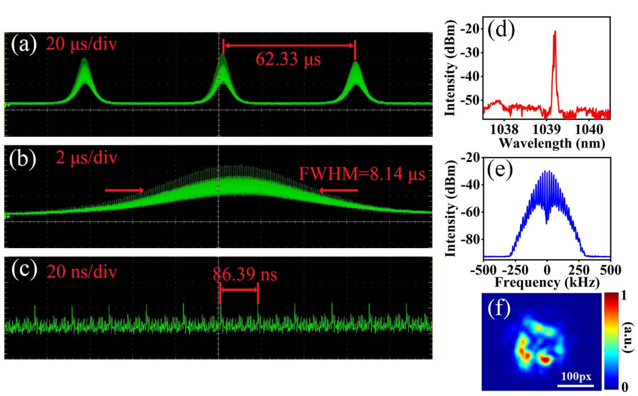

Fig. 3. QML operation at the pump power of 1.40 W. (a)–(c) QML pulse-train in the time range of 200 μs (20 μs/div), 20 μs (2 μs/div), and 200 ns (20 ns/div), respectively; (d) the corresponding optical spectrum; (e) the RF spectrum; (f) the beam profile.

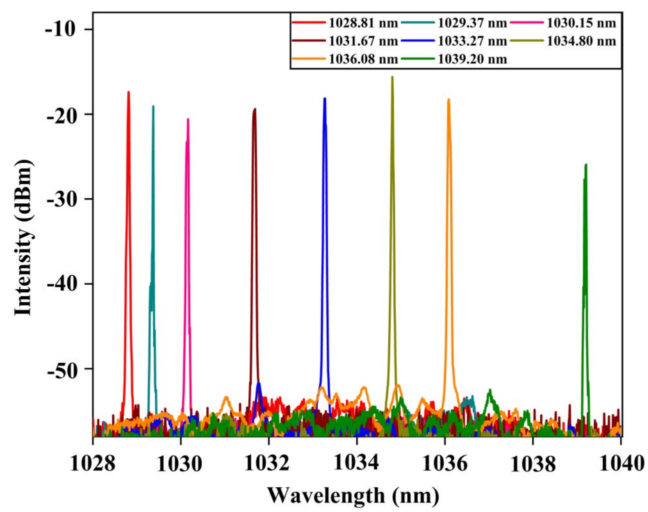

Fig. 4. Wavelength-tunable QML operation at the pump power of 1.40 W.

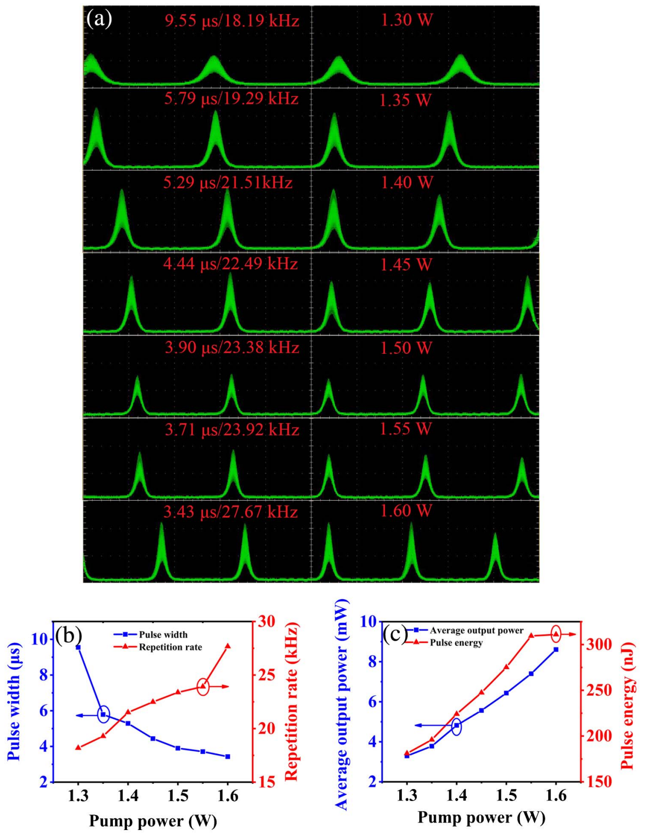

Fig. 5. Pump-dependent characteristics of the single-wavelength QML operation. (a) QML pulse-train under different pump power; (b) the pulse envelope width and repetition rate versus the pump power; (c) the average output power and pulse energy versus the pump power.

addition, the dependences of the average output power and the whole pulse envelope energy on the pump power are also measured and calculated, as depicted in Fig. 5(c). The maximum average output power and the maximum pulse envelope energy are 8.610 mW and 311.0 nJ at the pump power of 1.60 W, respectively. Note that the pulse energy only slightly increases when the pump power increases from 1.55 W to 1.60 W, which could be ascribed to the change of the operation state near the pump power of 1.60 W. In fact, the QML operation will be lost, and the laser emits a CW when we continue to increase the pump power to 1.65 W.

Particularly, we also observe harmonics in the Q-switched envelope. Figure 6 shows the characteristics of the QML operation with the fifth harmonic at the central wavelength of 1028.81 nm. Figure 6(a) shows the single QML pulse envelope, and the inset is the QML pulse-train on a larger time scale. The repetition rate and the pulse width of the Q-switched envelope are 23.87 kHz and 6.72 μs, respectively. The corresponding mode-locked pulses underneath the Q-switched envelope are illustrated in Fig. 6(b). The repetition rate of the mode-locked pulses is 57.97 MHz, corresponding to the fifth harmonic of the fundamental repetition rate of the cavity. It was demonstrated that harmonic mode-locked operation could be achieved by introducing appropriate highly nonlinear effects into the

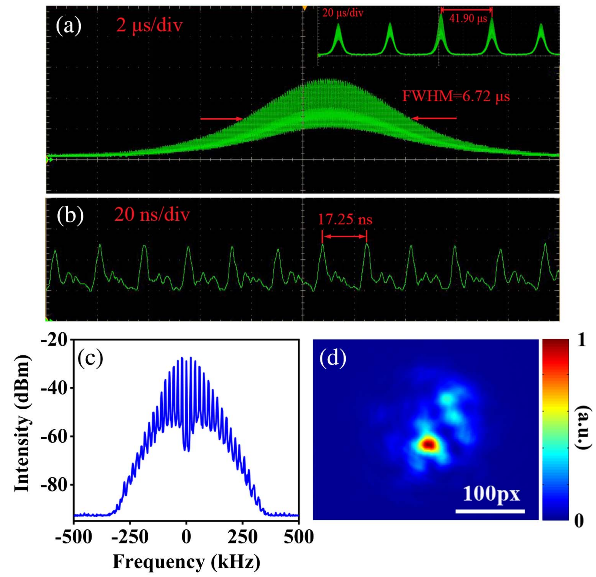

Fig. 6. Single-wavelength fifth harmonic QML operation at the pump power of 1.40 W. (a) The Q-switched envelope in the time range of 20 μs (2 μs/div), while the inset is the pulse-train in the time range of 200 μs (20 μs/div); (b) the mode-locked pulse-train underneath the Q-switched envelope in the time range of 200 ns (20 ns/div); (c) the RF spectrum; (d) the beam profile.

SMF laser cavity[42]. The generation of the fifth harmonic in the QML operation in our MMF laser could be attributed to the highly nonlinear effect caused by the GMM, since graphene has high nonlinearity, and the multimode microfiber also has high nonlinearity due to the decrease of the diameter[43]. The RF spectrum is also measured, as illustrated in Fig. 6(c). One can clearly see multiple frequency peaks with an interval of 23.87 kHz, corresponding to the repetition rate of the Q-switched pulse envelope. Besides, the corresponding output beam profile is presented in Fig. 6(d), which is still speckle.

3.2 Dual-wavelength QML operation

It is noted that in our MMF laser cavity, except for the GMM having a filtering effect, there is a few-mode fiber and MMF structure, which can form a filter and lead to the multiwavelength filtering effect[39]. Therefore, the dual-wavelength QML pulses could be obtained by adjusting the PCs in our experiment. Moreover, the spacing of the dual wavelength is tunable. Figure 7(a) displays the dual-wavelength lasing spectra with different spacings under the QML operations at the pump power of 1.40 W. The dual-wavelength spacing can be tuned from 0.93 nm to 5.79 nm by only adjusting the PCs. During the tuning process, the QML operation always remains stable. In addition, the variations in the spectral intensities and the existence of the satellite peaks are also observed, just like the ones observed in the single-wavelength QML operation in Fig. 4, which also arises from the differences of the loss and gain of these wavelengths. It should be pointed out that the dual-wavelength state could

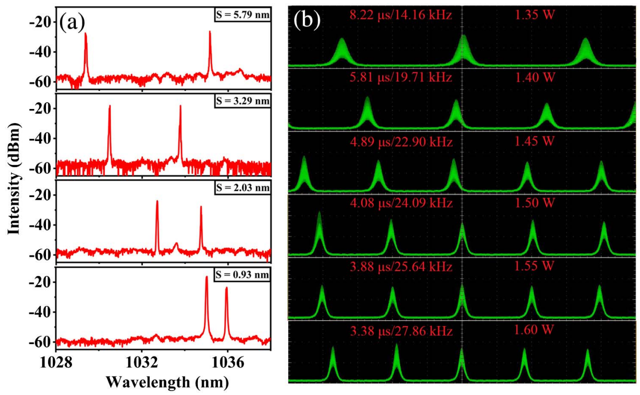

Fig. 7. Characteristics of the dual-wavelength QML operation. (a) The dual-wavelength spectra with different wavelength spacings at the pump power of 1.40 W; (b) the QML pulse-trains under different pump powers at the central wavelengths of 1030.48 nm and 1033.78 nm.

be switched to a single-wavelength QML state by finely adjusting the PCs. These tunable operations are due to the changing transmission of the filter based on the few-mode fiber and MMF structure and the GMM when manipulating the PCs.

Furthermore, we investigate the evolution of the pulse envelope with the pump power at the dual-wavelength QML states. With the increase of the pump power, the width of the Q-switched pulse envelope narrows, and the repetition rate increases, which are the same as that of the single-wavelength state. Figure 7(b) shows the evolution of the dual-wavelength QML pulses at the central wavelengths of 1030.48 nm and 1033.78 nm with the pump power. As seen from Fig. 7(b), the time interval between the adjacent Q-switched envelopes becomes shorter when the pump power is increased. The repetition rate can be tuned from 14.16 kHz to 27.86 kHz when the pump power rises from 1.35 W to 1.60 W. Meanwhile, the pulse envelope width decreases monotonously. The minimum pulse envelope width is 3.38 μs at the pump power of 1.60 W.

In this QML MMF laser, single-wavelength-tunable and dual-wavelength spacing-tunable operations can be realized. It increases the flexibility of the laser applications. Note that the tunable range of the single wavelength is only 10.39 nm, and the maximum spacing-tunable range of the dual wavelength is only 5.79 nm. This is mainly limited by the characteristics of the filter based on the few-mode fiber and MMF structure and the GMM filter. It could achieve a larger wavelength/wavelength-spacing-tunable range by optimizing the parameters of the filters, such as the length of the MMF[39]. It should be pointed out that in our experiments, when the PCs are slightly adjusted, the parameters of the QML pulse change little, which are similar to those of the initial QML state. However, when the PCs are drastically adjusted, the laser would lose the QML operation; thus, it needs to finely manipulate the PCs again to recover the QML state. At this time, the beam profiles of the QML states of the laser may be different since the adjustment of the PCs changes the excitation of the transverse modes. In addition, it is found that the quality of the mode-locked pulses underneath the Q-switched envelope in the QML operation is relatively poor, which could be ascribed to the large loss of the cavity. Nevertheless, our experimental results indicate that the temporal characteristics of the QML pulses generated in the MMF laser are similar to those of SMF lasers except for the beam profiles. Here, the beam profiles are speckle because of the existence of the multiple transverse modes in the cavity. However, it is difficult to further investigate the spatial mode characteristics of our QML MMF laser in our laboratory due to the immaturity of the measuring equipment and technologies. Similarly, the spatial characteristics of STML fiber lasers are also an issue to be solved. In recent years, many attempts were made to address this issue, for example, spatio-temporal-spectral compressed ultrafast photography (STS-CUP) technology[44] was employed to investigate the spatial characteristics of the STML solitons with different spectral components, while the multispeckle spectral-temporal (MUST) technology[45] was employed to study the spectral-temporal properties of the STML solitons in different speckle grains. Thus, with the development of the measuring equipment and technologies, more characteristics, especially the transverse modes characteristics of the pulses generated in MMF lasers, will be revealed. On the other hand, the beam quality is very important for laser applications. It is necessary to improve the beam quality in MMF lasers. Nevertheless, it is also difficult. At present, it may be improved through the beam Kerr self-cleaning effect[27]. In the future, other techniques are expected to be developed.

In our experiments, QML operation can be achieved by using different GMMs with waist diameters from 4.16 μm to 14.04 μm and modulation depths from 21.82% to 37.90%. However, the STML operation is unable to be achieved in our laser with these GMMs. Generally, the non-saturable loss of the saturable absorber increases as its modulation depth increases, and the relatively large loss is conducive to realizing the QML operation. Thus, we think that the main reason is that the modulation depths of the GMMs used in our laser are too large, which is accompanied with a relatively large non-saturable loss. In addition to the large modulation depth/non-saturable loss of the GMMs, another reason is that the splice losses of the cavity are too large since the different types of fibers are used in our laser. Thus, to achieve the STML operation in the future work, it is necessary to optimize the parameters of the fabricated GMM, such as the modulation depth and the non-saturable loss, and further reduce the loss of the cavity.

4. Conclusion

In conclusion, we report the QML pulses generation in an Yb-doped MMF fiber laser by using a GMM. Due to the filtering effect induced by the few-mode fiber and MMF structure and the GMM in the cavity, both the single-wavelength and dual-wavelength QML pulses are obtained by adjusting the PCs. Moreover, the central wavelength of the single-wavelength QML operation can be tuned from 1028.81 nm to 1039.20 nm, and the spacing of the dual-wavelength QML operation can be tuned from 0.93 nm to 5.79 nm. The obtained results indicate that QML pulses can be produced in the MMF laser, and such a flexible and functional laser would contribute to the application in fields of optical sensing, laser measuring, and processing.

Acknowledgement

This work was supported by the National Natural Science Foundation of China (Nos. 92050101, 61875058, 11874018, 11974006, and 61378036) and the Natural Science Foundation of Guangdong Province (No. 2021A1515011608).

References

1. D. J. Richardson, J. M. Fini, and L. E. Nelson, "Space-division multiplexing in optical fibres," Nat. Photon. **7**, 354 (2013).
2. H. R. Stuart, "Dispersive multiplexing in multimode optical fiber," Science **289**, 281 (2000).
3. D. J. Richardson, J. Nilsson, and W. A. Clarkson, "High power fiber lasers: current status and future perspectives [Invited]," J. Opt. Soc. Am. B **27**, B63 (2010).
4. I. N. Papadopoulos, S. Farahi, C. Moser, and D. Psaltis, "High-resolution, lensless endoscope based on digital scanning through a multimode optical fiber," Biomed. Opt. Express **4**, 260 (2013).
5. M. Plöschner, T. Tyc, and T. Čižmár, "Seeing through chaos in multimode fibres," Nat. Photon. **9**, 529 (2015).
6. I. Barmes, S. Witte, and K. S. E. Eikema, "Spatial and spectral coherent control with frequency combs," Nat. Photon. **7**, 38 (2013).
7. H. Defienne, M. Barbieri, I. A. Walmsley, B. J. Smith, and S. Gigan, "Two-photon quantum walk in a multimode fiber," Sci. Adv. **2**, e1501054 (2016).
8. B. Redding and H. Cao, "Using a multimode fiber as a high-resolution, low-loss spectrometer," Opt. Lett. **37**, 3384 (2012).
9. L. G. Wright, S. Wabnitz, D. N. Christodoulides, and F. W. Wise, "Ultrabroadband dispersive radiation by spatiotemporal oscillation of multimode waves," Phys. Rev. Lett. **115**, 223902 (2015).
10. L. G. Wright, D. N. Christodoulides, and F. W. Wise, "Controllable spatiotemporal nonlinear effects in multimode fibres," Nat. Photon. **9**, 306 (2015).
11. K. Krupa, A. Tonello, A. Barthélémy, V. Couderc, B. M. Shalaby, A. Bendahmane, G. Millot, and S. Wabnitz, "Observation of geometric parametric instability induced by the periodic spatial self-imaging of multimode waves," Phys. Rev. Lett. **116**, 183901 (2016).
12. R. Dupiol, A. Bendahmane, K. Krupa, A. Tonello, M. Fabert, B. Kibler, T. Sylvestre, A. Barthelemy, V. Couderc, S. Wabnitz, and G. Millot, "Far-detuned cascaded intermodal four-wave mixing in a multimode fiber," Opt. Lett. **42**, 1293 (2017).
13. U. Teğin and B. Ortaç, "Spatiotemporal instability of femtosecond pulses in graded-index multimode fibers," IEEE Photon. Tech. Lett. **29**, 2195 (2017).
14. G. Lopez-Galmiche, Z. Sanjabi Eznaveh, M. A. Eftekhar, J. Antonio Lopez, L. G. Wright, F. Wise, D. Christodoulides, and R. A. Correa, "Visible supercontinuum generation in a graded index multimode fiber pumped at 1064 nm," Opt. Lett. **41**, 2553 (2016).
15. K. Krupa, C. Louot, V. Couderc, M. Fabert, R. Guenard, B. M. Shalaby, A. Tonello, D. Pagnoux, P. Leproux, A. Bendahmane, R. Dupiol, G. Millot, and S. Wabnitz, "Spatiotemporal characterization of supercontinuum extending from the visible to the mid-infrared in a multimode graded-index optical fiber," Opt. Lett. **41**, 5785 (2016).
16. M. A. Eftekhar, L. G. Wright, M. S. Mills, M. Kolesik, R. A. Correa, F. W. Wise, and D. N. Christodoulides, "Versatile supercontinuum generation in parabolic multimode optical fibers," Opt. Express **25**, 9078 (2017).
17. K. Krupa, A. Tonello, V. Couderc, A. Barthélémy, G. Millot, D. Modotto, and S. Wabnitz, "Spatiotemporal light-beam compression from nonlinear mode coupling," Phys. Rev. A **97**, 043836 (2018).
18. K. Krupa, A. Tonello, B. M. Shalaby, M. Fabert, A. Barthélémy, G. Millot, S. Wabnitz, and V. Couderc, "Spatial beam self-cleaning in multimode fibres," Nat. Photon. **11**, 237 (2017).
19. L. G. Wright, Z. Liu, D. A. Nolan, M.-J. Li, D. N. Christodoulides, and F. W. Wise, "Self-organized instability in graded-index multimode fibres," Nat. Photon. **10**, 771 (2016).
20. Z. Liu, L. G. Wright, D. N. Christodoulides, and F. W. Wise, "Kerr self-cleaning of femtosecond-pulsed beams in graded-index multimode fiber," Opt. Lett. **41**, 3675 (2016).
21. R. Guenard, K. Krupa, R. Dupiol, M. Fabert, A. Bendahmane, V. Kermene, A. Desfarges-Berthelemot, J. L. Auguste, A. Tonello, A. Barthélémy, G. Millot, S. Wabnitz, and V. Couderc, "Kerr self-cleaning of pulsed beam in an ytterbium doped multimode fiber," Opt. Express **25**, 4783 (2017).
22. E. Deliancourt, M. Fabert, A. Tonello, K. Krupa, A. Desfarges-Berthelemot, V. Kermene, G. Millot, A. Barthélémy, S. Wabnitz, and V. Couderc, "Kerr beam self-cleaning on the LP_{11} mode in graded-index multimode fibers," OSA Continuum **2**, 1089 (2019).
23. B. Morasse, S. Chatigny, C. Desrosiers, É. Gagnon, M.-A. Lapointe, and J.-P. De, "Simple design for singlemode high power CW fiber laser using multimode high NA fiber," Proc. SPIE **7195**, 719505 (2009).
24. L. Li, Q. Lou, J. Zhou, J. Dong, Y. Wei, and J. Li, "High power low-order modes operation of a multimode fiber laser," Chin. Opt. Lett. **5**, 221 (2007).
25. L. G. Wright, D. N. Christodoulides, and F. W. Wise, "Spatiotemporal mode-locking in multimode fiber lasers," Science **358**, 94 (2017).
26. U. Teğin, B. Rahmani, E. Kakkava, D. Psaltis, and C. Moser, "All-fiber spatiotemporally mode-locked laser with multimode fiber-based filtering," Opt. Express **28**, 23433 (2020).
27. U. Teğin, B. Rahmani, E. Kakkava, D. Psaltis, and C. Moser, "Single-mode output by controlling the spatiotemporal nonlinearities in mode-locked femtosecond multimode fiber lasers," Adv. Photon. **2**, 056005 (2020).
28. Y. Ding, X. Xiao, K. Liu, S. Fan, X. Zhang, and C. Yang, "Spatiotemporal mode-locking in lasers with large modal dispersion," Phys. Rev. Lett. **126**, 093901 (2021).
29. Y. Ding, X. Xiao, P. Wang, and C. Yang, "Multiple-soliton in spatiotemporal mode-locked multimode fiber lasers," Opt. Express **27**, 11435 (2019).
30. H. Qin, X. Xiao, P. Wang, and C. Yang, "Observation of soliton molecules in a spatiotemporal mode-locked multimode fiber laser," Opt. Lett. **43**, 1982 (2018).
31. U. Teğin, E. Kakkava, B. Rahmani, D. Psaltis, and C. Moser, "Spatiotemporal self-similar fiber laser," Optica **6**, 1412 (2019).
32. K. Liu, X. Xiao, X. Zhang, and C. Yang, "Multimode *Q*-switching and spatiotemporal mode-locking in multimode fiber lasers," in *Conference on Lasers and Electro-Optics* (2020), paper SM4P.2.
33. R. Miao, M. Tong, K. Yin, H. Ouyang, Z. Wang, X. Zheng, X. A. Cheng, and T. Jiang, "Soliton mode-locked fiber laser with high-quality MBE-grown Bi_2Se_3 film," Chin. Opt. Lett. **17**, 071403 (2019).
34. H. Gu, Z. Qin, G. Xie, T. Hai, P. Yuan, J. Ma, and L. Qian, "Generation of 131 fs mode-locked pulses from 2.8 μm Er:ZBLAN fiber laser," Chin. Opt. Lett. **18**, 031402 (2020).
35. P. Cheng, Y. Du, M. Han, and X. Shu, "Mode-locked and *Q*-switched mode-locked fiber laser based on a ferroferric-oxide nanoparticles saturable absorber," Opt. Express **28**, 13177 (2020).
36. U. Chakravarty, S. Gurram, A. Kuruvilla, B. N. Upadhyaya, and K. S. Bindra, "Short pulse generation in active *Q*-switched Yb-doped all fiber laser and its amplification," Opt. Laser Technol. **109**, 186 (2019).
37. Z.-C. Luo, M. Liu, H. Liu, X.-W. Zheng, A.-P. Luo, C.-J. Zhao, H. Zhang, S.-C. Wen, and W.-C. Xu, "2 GHz passively harmonic mode-locked fiber laser by a microfiber-based topological insulator saturable absorber," Opt. Lett. **38**, 5212 (2013).
38. K. Kieu and M. Mansuripur, "Tuning of fiber lasers by use of a single-mode biconic fiber taper," Opt. Lett. **31**, 2435 (2006).
39. J.-G. Long, Y.-X. Gao, W. Lin, J.-W. Wu, X.-B. Lin, W.-Y. Hong, H. Cui, Z.-C. Luo, W.-C. Xu, and A.-P. Luo, "Switchable and spacing tunable dual-wavelength spatiotemporal mode-locked fiber laser," Opt. Lett. **46**, 588 (2021).
40. T. Hakulinen and O. G. Okhotnikov, "8 ns fiber laser *Q* switched by the resonant saturable absorber mirror," Opt. Lett. **32**, 2677 (2007).
41. J. J. Zayhowski and P. L. Kelley, "Optimization of *Q*-switched lasers," IEEE J. Quantum Electron. **27**, 2220 (1991).

42. C. S. Jun, S. Y. Choi, F. Rotermund, B. Y. Kim, and D.-I. Yeom, “Toward higher-order passive harmonic mode-locking of a soliton fiber laser,” Opt. Lett. **37**, 1862 (2012).
43. Y.-L. Qi, H. Liu, H. Cui, Y.-Q. Huang, Q.-Y. Ning, M. Liu, Z.-C. Luo, A.-P. Luo, and W.-C. Xu, “Graphene-deposited microfiber photonic device for ultrahigh-repetition rate pulse generation in a fiber laser,” Opt. Express **23**, 17720 (2015).
44. J. C. Jing, X. Wei, and L. V. Wang, “Spatio-temporal-spectral imaging of non-repeatable dissipative soliton dynamics,” Nat. Commun. **11**, 2059 (2020).
45. Y. Guo, X. Wen, W. Lin, W. Wang, X. Wei, and Z. Yang, “Real-time multi-speckle spectral-temporal measurement unveils the complexity of spatiotemporal solitons,” Nat. Commun. **12**, 67 (2021).